Dissipative discrete breathers: Periodic, quasiperiodic, chaotic, and mobile

P. J. Martínez
Departamento de Teoría y Simulación de Sistemas Complejos, Instituto de Ciencia de Materiales de Aragón, C.S.I.C.-Universidad de Zaragoza, 50009 Zaragoza, Spain; Departamento de Física Aplicada, Universidad de Zaragoza, 50009 Zaragoza, Spain; and Instituto de Biocomputación y Física de Sistemas Complejos, Universidad de Zaragoza, 50009 Zaragoza, Spain

M. Meister
Departamento de Teoría y Simulación de Sistemas Complejos, Instituto de Ciencia de Materiales de Aragón, C.S.I.C.-Universidad de Zaragoza, 50009 Zaragoza, Spain and Departamento de Física de la Materia Condensada, Universidad de Zaragoza, 50009 Zaragoza, Spain

L. M. Floría and F. Falo
Departamento de Teoría y Simulación de Sistemas Complejos, Instituto de Ciencia de Materiales de Aragón, C.S.I.C.-Universidad de Zaragoza, 50009 Zaragoza, Spain; Departamento de Física de la Materia Condensada, Universidad de Zaragoza, 50009 Zaragoza, Spain; and Instituto de Biocomputación y Física de Sistemas Complejos, Universidad de Zaragoza, 50009 Zaragoza, Spain

(Received 7 October 2002; accepted 13 January 2003; published 22 May 2003)

The properties of discrete breathers in dissipative one-dimensional lattices of nonlinear oscillators subject to periodic driving forces are reviewed. We focus on oscillobreathers in the Frenkel–Kontorova chain and rotobreathers in a ladder of Josephson junctions. Both types of exponentially localized solutions are easily obtained numerically using adiabatic continuation from the anticontinuous limit. Linear stability (Floquet) analysis allows the characterization of different types of bifurcations experienced by periodic discrete breathers. Some of these bifurcations produce nonperiodic localized solutions, namely, quasiperiodic and chaotic discrete breathers, which are generally impossible as exact solutions in Hamiltonian systems. Within a certain range of parameters, propagating breathers occur as attractors of the dissipative dynamics. General features of these excitations are discussed and the Peierls–Nabarro barrier is addressed. Numerical scattering experiments with mobile breathers reveal the existence of two-breather bound states and allow a first glimpse at the intricate phenomenology of these special multibreather configurations. © *2003 American Institute of Physics.* [DOI: 10.1063/1.1557237]

Discrete breathers in dissipative arrays of nonlinear oscillators with periodic forcing show a remarkably rich variety of behaviors, compared to Hamiltonian discrete breathers. Nonperiodic localized solutions in Hamiltonian lattices would decay due to the unavoidable emission of phonons which delocalize the breather energy. This also explains why Hamiltonian mobile breathers can only be numerically observed as (long-lived) transients. However, as we will see here, quasiperiodic, chaotic, and mobile discrete breathers appear as exact solutions in dissipative lattices due to the efficient damping of the radiation away from the breather center.

I. INTRODUCTION

The aim of this contribution is to review some recent work on intrinsic localized modes (discrete breathers) in dissipative systems of nonlinear oscillators subjected to periodic driving forces. Because of their fundamental interest, Hamiltonian discrete breathers have received much more attention than their dissipative counterparts. On the other hand, experimental systems (like Josephson junction arrays) where discrete breathers (DB) can be observed are often dissipative, and this adds considerable interest to the study of the subject.

The mathematical proofs of existence of discrete breathers in Hamiltonian networks of nonlinear oscillators[1] requires that a condition of nonresonance of the localized oscillation (or rotation) with the band of extended oscillations of small amplitude (normal modes) of the lattice has to be satisfied. However, this condition is not required for the existence of discrete breathers in general dissipative networks of oscillators.[2,3] Moreover, as explicitly proved in Ref. 4 the dissipative breather possesses the character of attractor for initial conditions in the corresponding basin of attraction. Roughly speaking, normal modes in dissipative lattices are exponentially damped out, and thus the exponential localization of energy is not destroyed by the resonance of the DB harmonics with the ''phonon band.'' On one hand, this makes considerably easier the numerical computation of dissipative DB's and on the other, as we will show below, it allows for the existence of quasiperiodic and even chaotic DB's, a fact that is in principle excluded for Hamiltonian systems.

We mainly consider here two different examples of DB's in dissipative lattices: Oscillobreathers in the standard Frenkel–Kontorova model with the commensurability one

(i.e., average interparticle distance equal to the period of the sinusoidal substrate potential), and rotobreathers in an anisotropic ladder of Josephson junctions with injected ac currents. Though very briefly, we will also make some mention to an example of discrete breather in a simple model of coupled Van der Pol oscillators. In Sec. II we discuss briefly the numerical procedures used to obtain accurate breather solutions in both models, which are based on the continuation from the uncoupled limit of each model.

In Sec. III we explain some general features of the linear stability (Floquet) analysis of forced-damped periodic DB. Intended to be self-contained (to some extent), this section deals with both models, which due to some remarkable differences in the damping terms present some different features in their linear stability analysis. After deriving some straightforward properties of the Floquet multipliers, we obtain some formal conditions for the nonappearance of extended instabilities of the uniformly oscillating background, along with the tail analysis valid for not-too-large forcing.

In Sec. IV we review the phase diagrams of pinned (nonmobile) DB in the Frenkel–Kontorova model and the Josephson junction ladder. In both models we find different bifurcations experienced by the periodic DB. Interestingly, some of these bifurcations produce nonperiodic types of localized solutions, like quasiperiodic and chaotic discrete breathers. We have analyzed their behaviors with different techniques (Lyapunov exponents, Poincaré sections, etc.) which unambiguously confirm the localized character of those excitations.

In Sec. V we turn our attention to mobile DB, i.e., discrete breathers propagating through the system. These excitations have been observed both in Hamiltonian and dissipative systems. In this report, our focus is on the later case, in particular on the forced-damped Frenkel–Kontorova (FK) model. After some general remarks, we discuss the Peierls–Nabarro barrier for mobile breathers. Then we recall some recent results on mobile breathers in the FK model before we turn to the interaction of mobile discrete breathers in scattering processes. The most interesting outcome of a two-breather scattering process is a bound state. About these states little is known so far. We present the results of a larger number of scattering processes, providing first insights into the rich phenomenology of these mobile multibreather states.

II. MODELS AND NUMERICAL PROCEDURES

A. The Frenkel–Kontorova model

The Frenkel–Kontorova model of classical, harmonically coupled, atoms experiencing a substrate sinusoidal potential, was introduced more than 60 years ago[5] to study the structure and dynamics of dislocations in metals. Along the subsequent decades it has become one of the most universal models of nonlinear physics, often used to investigate a rather broad set of physical phenomena and systems like charge (or spin) density waves, adsorbed monolayers on surfaces, commensurate–incommensurate transitions, dry friction, Josephson junction arrays, to name a few of them.[6,7] The equations of motion of the Frenkel–Kontorova chain subject to damping and an (spatially uniform) external driving force are, in dimensionless form,

$$\ddot{u}_j+\alpha\dot{u}_j+\frac{1}{2\pi}\sin(2\pi u_j)=C(u_{j+1}-2u_j+u_{j-1})+F_{ac}\sin(\omega_b t). \quad (1)$$

In order to generate a DB configuration we start in the uncoupled limit $C=0$, that is, we first consider the dynamics of a single forced and damped pendulum, and try to find a region of parameters where there are at least two different attractors (oscillations) coexisting. Note that, generically, all oscillators have at least two attractors for sufficiently low values of the damping α and the force F_{ac}, if the frequency ω_b of the force is not wildly different from the typical frequencies of the autonomous oscillator.

Therefore we initially choose values for α, F_{ac}, and ω_b, and keep them fixed while we vary C. Then, for instance, we fix one of the oscillators to the high amplitude solution and all the others to the low one. Using as initial condition this uncoupled configuration, we turn on adiabatically the coupling parameter C. The initial solution can be continued for $C\neq 0$ (Refs. 2, 3) and it is assured that the continued solution is an attractor of the dynamics.[4] Moreover, as one expects that the basins of attraction evolve continuously with C as well, if the variation in C is small enough, this initial condition is expected to evolve to the stable attractor, i.e., the exact continued DB. This makes the numerical continuation much simpler than in the case of Hamiltonian systems, where expensive root-finding methods are needed for breather continuation.[8]

The numerical integration of equations of motion has been done using a fourth-order Runge–Kutta method. The parameters that we have mostly used in the simulations shown below are $\alpha=0.02$, $\omega_b=0.2\pi$, and $F_{ac}=0.02$. Simulations for different values of the parameters were also performed, in order to confirm the general validity of our results. Though not in a systematic manner, in some generic cases we have added to the initial conditions a small random noise (typically of order 10^{-5}) to test for robustness. Moreover, special care has been taken in dealing with finite size effects. While for low values of C ($C<0.6$) small lattice sizes can be used (say $N=40$), once the breather is dressed by a phonon tail (see Sec. III C), one needs to increase the lattice size (sometimes up to $N=900$) in order to avoid finite size effects. Both, coupling to a noise source and finite size effects are important issues on their own, not only from a simulational and theoretical point of view, since experiments in real dissipative systems are often done in small lattices[9,10] which are in contact (both thermal and nonthermal) with a variety of degrees of freedom.

B. The Josephson junction ladder

Rotobreathers are DB's in which one (or more) central oscillator rotates and the rest oscillate with decaying amplitude. The amplitude of tail oscillations decay to zero in Hamiltonian rotobreathers while for periodically forced systems they decay to the uniformly oscillating solution of the

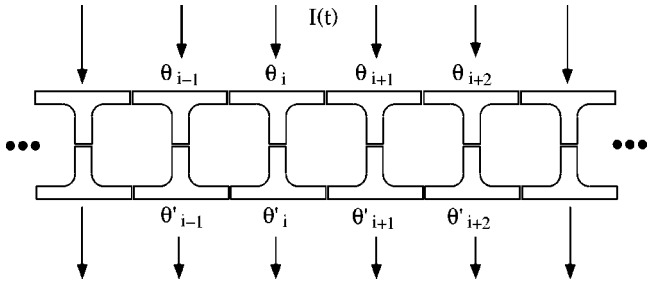

FIG. 1. Schematic picture of the Josephson junction ladder biased by ac currents injected as shown.

forced and damped lattice. This kind of DB cannot exist in, for example, the Frenkel–Kontorova model, for the coupling energy between a rotating oscillator and its oscillating neighbor would diverge quickly as time evolves. The coupling term has clearly to be a bounded function of the variable increment. But this is the case for many realistic models in condensed matter systems, like Heisenberg or XY classical spin models, where interactions are sinusoidal.

Rotobreathers were first numerically found by Takeno and Peyrard,[11] who also worked out approximate analytical expressions[12] for a Hamiltonian system of sinusoidally coupled rotators. The existence proof of rotobreathers can be said to be implicitly envisaged in the seminal work of Mackay and Aubry,[1] and it was later explicitly considered in Refs. 2 and 4.

A system where rotobreathers were predicted[4,13] and, indeed, experimentally observed[9,10,14] is the anisotropic Josephson ladder, where two rows of superconducting islands (see Fig. 1) are interconnected through vertical and horizontal Josephson junctions (each type having different junction characteristic parameters, subindexed by y and x below). Under the appropriate circumstances (see Refs. 13 and 15 for relevant details) the so-called resistively and capacitively shunted junction (RCSJ) approximation provides an excellent description of the array dynamics in terms of the superconducting phases θ_i (and θ_i') of the upper (and lower) islands.

The equations of motion in the RCSJ framework are

$$\ddot{\chi}_i = J_x[\sin(\chi_{i+1}-\chi_i)\cos(\phi_{i+1}-\phi_i)+\sin(\chi_{i-1}-\chi_i) \times\cos(\phi_{i-1}-\phi_i)]+\epsilon_x(\dot{\chi}_{i+1}+\dot{\chi}_{i-1}-2\dot{\chi}_i), \tag{2}$$

$$\ddot{\phi}_i = J_x[\cos(\chi_{i+1}-\chi_i)\sin(\phi_{i+1}-\phi_i)+\cos(\chi_{i-1}-\chi_i) \times\sin(\phi_{i-1}-\phi_i)]+\epsilon_x(\dot{\phi}_{i+1}+\dot{\phi}_{i-1}-2\dot{\phi}_i) -J_y\sin(2\phi_i)-2\epsilon_y\dot{\phi}_i-I(t), \tag{3}$$

where $\chi_i=\frac{1}{2}(\theta_i+\theta_i')$ and $\phi_i=\frac{1}{2}(\theta_i-\theta_i')$, $I(t)=I_{ac}\cos(\omega t)$ is the uniform bias current, $J_{x,y}$ are the Josephson couplings (or critical currents) of junctions in the horizontal (x) and vertical (y) links, and $\epsilon_{x,y}$ incorporate the resistive effects from the contribution of normal electrons in the (respectively horizontal and vertical) junctions.

Equation (2) can be effectively decoupled from Eq. (3) by choosing uniform initial conditions in the "center-of-mass" coordinates (i.e., χ_i and $\dot{\chi}_i$ independent of i). For these initial conditions, Eq. (2) has the solution $\chi_i(t)=\Omega t+\beta$ for all i, where Ω and β can be chosen zero by a judicious choice of the uniform initial conditions $\chi_i(0),\dot{\chi}_i(0)$. One can then focus attention on the ϕ_i variables (though not exclusively, for one has to check for stability of the χ-homogeneous solution, see below).

In order to generate the rotobreather solution, we look for values of the parameters $(J_y,\epsilon_y,I_{ac},\omega)$ of the decoupled pendulum ϕ (i.e., $J_x=\epsilon_x=0$) for which rotating and oscillating attractors coexist. Then we fix one of the oscillators to the rotating solution and all the rest to the oscillating one, and keeping fixed $(J_y,\epsilon_y,I_{ac},\omega)$ while varying J_x and ϵ_x, proceed to the continuation of the rotobreather solution. As argued in the previous subsection, adiabatic variation of the couplings and integration of the equations of motion (2) and (3) is all that is needed, due to the attractor character of the rotobreather solution. Most of the results shown below were computed for $J_y=0.5$ and $\epsilon_y=0.01$, while the other parameters were varied inside some adequate ranges of values. As with the case in the previous subsection, both finite size effects and robustness against small random noise were carefully checked.

III. LINEAR STABILITY ANALYSIS

A. Floquet multipliers

Let us denote by $\{u_j(t)\}$ the periodic DB solution of the Frenkel–Kontorova model (1) which is numerically continued from the uncoupled limit, and consider a small perturbation, $\{v_j(t)\}$, with $v_j=u_j+\epsilon_j$. After discarding terms which are nonlinear in ϵ_j (assumed to be small) one obtains the linearized equations of motion around the DB solution,

$$\ddot{\epsilon}_j+\alpha\dot{\epsilon}_j+\cos(2\pi u_j(t))\epsilon_j=C(\epsilon_{j+1}-2\epsilon_j+\epsilon_{j-1}). \tag{4}$$

Note that $u_j(t)$ are periodic functions of time of period $t_b=2\pi/\omega_b$, so that, for a system of size N, Eqs. (4) forms a system of N coupled linear differential equations with time periodic coefficients. If $\{\epsilon_j(0),\dot{\epsilon}_j(0)\}$ denote a basis of initial conditions in the $2N$-dimensional tangent space, the monodromy (or Floquet) matrix $\mathcal{F}$ is obtained by integration of the linearized Eq. (4) over a period t_b for each of the $2N$ basis vectors,

$$\begin{pmatrix}\epsilon_j(t_b)\\ \dot{\epsilon}_j(t_b)\end{pmatrix}=\mathcal{F}\begin{pmatrix}\epsilon_j(0)\\ \dot{\epsilon}_j(0)\end{pmatrix}. \tag{5}$$

The Floquet matrix $\mathcal{F}$ relates the small perturbations at $t=t_b$ to those at $t=0$; in other words, $\mathcal{F}$ is the matrix associated to the (linear) t_b-map of (4).

In a similar way, one obtains the linearized equations of motion around the ladder rotobreather solution $\{\chi_i(t)=0,\phi_i\}$,

$$\delta\ddot{\chi}_i = J_x[\cos(\phi_{i+1}-\phi_i)(\delta\chi_{i+1}-\delta\chi_i)+\cos(\phi_{i-1}-\phi_i) \times(\delta\chi_{i-1}-\delta\chi_i)]+\epsilon_x[\delta\dot{\chi}_{i+1}+\delta\dot{\chi}_{i-1}-2\delta\dot{\chi}_i], \tag{6}$$

$$\delta\ddot{\phi}_i = J_x[\cos(\phi_{i+1}-\phi_i)(\delta\phi_{i+1}-\delta\phi_i)+\cos(\phi_{i-1}-\phi_i) \times(\delta\phi_{i-1}-\delta\phi_i)]+\epsilon_x[\delta\dot{\phi}_{i+1}+\delta\dot{\phi}_{i-1}-2\delta\dot{\phi}_i] -2J_y\cos(2\phi_i)\delta\phi_i-2\epsilon_y\delta\dot{\phi}_i, \tag{7}$$

and by integration over a period $T_b=2\pi/\omega_b=4\pi/\omega$ of a vector basis in the ($4N$-dimensional) tangent space $\{\delta\chi_i,\delta\phi_i,\delta\dot{\chi}_i,\delta\dot{\phi}_i\}$, the Floquet matrix $\mathcal{F}$ is obtained,

$$\{\delta\chi_i,\delta\phi_i,\delta\dot{\chi}_i,\delta\dot{\phi}_i\}^T_{t=T_b}=\mathcal{F}\{\delta\chi_i,\delta\phi_i,\delta\dot{\chi}_i,\delta\dot{\phi}_i\}^T_{t=0}. \quad (8)$$

The linear stability of the breather solution (either $\{u_j(t)\}$ or $\{\chi_i(t)=0,\phi_i(t)\}$) requires that all the eigenvalues of the corresponding Floquet matrix (called *Floquet multipliers*) are inside the unit circle. The corresponding eigenvectors are the directions along which the perturbations grow or decay with a rate given by the Floquet multipliers. Since $\mathcal{F}$ is real, if μ is an eigenvalue of $\mathcal{F}$, its complex conjugate $\overline{\mu}$ is also an eigenvalue of $\mathcal{F}$.

For the case of the Frenkel–Kontorova model the Floquet spectrum has a special structure, whose details are revealed using the transformation (see Ref. 16)

$$\epsilon_j(t)=e^{-\alpha t/2}\eta_j(t), \quad (9)$$

which transforms the linear dissipative system of Eq. (4) into a (nonautonomous) Hamiltonian system of oscillators,

$$\ddot{\eta}_j-(\alpha^2/4-\cos(2\pi u_j(t)))\,\eta_j=C(\eta_{j+1}-2\eta_j+\eta_{j-1}). \quad (10)$$

The eigenvalues of the linear symplectic t_b-map of these equations must come in pairs such that their product is unity. Together with the fact that the map is real, one has these well known[17] three possible cases: (i) pairs of complex conjugate eigenvalues lying on the unit circle, with $\lambda_1=\overline{\lambda}_2$; (ii) pairs lying on the real axis, with $\lambda_1=1/\lambda_2$; (iii) 4-tuples of eigenvalues with $\lambda_1=1/\lambda_2=\overline{\lambda}_3=1/\overline{\lambda}_4$. Note that the transformation (9) scales the eigenvalues by a factor $\exp[-\alpha t_b/2]$, and thus the Floquet multipliers of (4) must either lie on a circle of radius $\exp(-\alpha t_b/2)$, with $\mu_1=\overline{\mu}_2$, or on the real axis such that $\mu_1\mu_2=\exp(-\alpha t_b)$, or come as 4-tuples such that $\mu_1=\overline{\mu}_3$, $\mu_2=\overline{\mu}_4$, $\mu_1=\exp(-\alpha t_b)/\overline{\mu}_4$.

On the contrary, the Floquet spectrum of the ladder rotobreather does not have such ''almost-symplectic'' structure, because of the damping terms in the form of (discrete) Laplacians of the velocities which appear in the linearized Eqs. (6) and (7). This type of damping term, sometimes referred to as ''phonon damping,'' imposes different decaying time scales to normal modes of different wave vector (see next subsection), thus producing a more scattered structure of Floquet multipliers in the complex plane.

B. Extended instabilities

In the limit of an infinite system ($N\to\infty$), the Floquet spectrum of a breather consists of a continuous part associated with spatially extended eigenvectors and a discrete part associated with spatially localized eigenvectors. Marín and Aubry[18] have argued that the continuous part of the spectrum of $\mathcal{F}$ is the continuous spectrum of the Floquet matrix $\mathcal{F}_0$ of the linearized problem around the homogeneous solution (i.e., without breather) $\{u_j(t)\}=\{u_\infty(t)\}$ (FK model) or $\{\chi_i(t)=0,\phi_i(t)\}=\{0,\phi_\infty(t)\}$ (Josephson ladder).

First, we consider the spectrum of $\mathcal{F}_0$ for the Frenkel–Kontorova model. Under the usual periodic boundary conditions, we look for solutions of the linear problem with the plane-wave form $\eta_j(t)=e^{iqj}\eta^q(t)$. Denoting simply by $f(t)=\cos(2\pi u_\infty(t))$, and $E(q)=4C\sin^2(q/2)-\alpha^2/4$, we obtain for each spatial Fourier coefficient $\eta^q(t)$ the equation

$$\ddot{\eta}^q(t)+(E(q)+f(t))\,\eta^q(t)=0. \quad (11)$$

This is a Hill equation. For each solution $\eta^q(t)$ of the single Hill equation (11) we have a solution of the form,

$$\epsilon_j(t)=e^{iqj}e^{-\alpha t/2}\eta^q(t) \quad (12)$$

for the linearized problem. The Hill equation (11) has a general solution which can be expressed in terms of its *normal solutions*, which have the property,

$$\eta^q(t+2\pi/\omega_b)=\lambda_q\eta^q(t), \quad (13)$$

where λ_q is called the characteristic number of the equation. The complex number ρ_q defined as $\lambda_q=\exp(2\pi\rho_q/\omega_b)$ is called characteristic exponent (its imaginary part being defined up to an additive multiple of ω_b). In the generic case in which Eq. (11) has two different characteristic numbers λ_q^+,λ_q^-, their product is equal to unity, $\lambda_q^+\lambda_q^-=1$, and the general solution has the form

$$\eta^q(t)=c_+e^{\rho_q^+t}\psi_q^+(t)+c_-e^{\rho_q^-t}\psi_q^-(t), \quad (14)$$

where c_+,c_- are constants and ψ_q^+,ψ_q^- are time periodic functions with period $2\pi/\omega_b$. Consequently, $\eta^q(t)$ is bounded by $K\exp(\rho_q^{\max}t)$, with K some constant, and $\rho_q^{\max}=\max\{\rho_q^+,\rho_q^-\}$. Thus, from Eq. (12), we conclude that the stability of the homogeneous solution $\{u_\infty(t)\}$ is assured in the parameter region in which

$$\rho_{\sup}=\sup_q\rho_q^{\max}<\alpha/2. \quad (15)$$

The determination of this region in parameter space can only be done by numerical means. For the range of parameters that we have used in our studies, the function $f(t)$ is a low amplitude oscillation around the value 1, and, as expected from the well-known results on weakly time dependent Hill equations, we have not observed instabilities by extended modes.

Now we consider the spectrum of $\mathcal{F}_0$ for the ladder. The linearized equations of motion around the homogeneous solution are, for the $\{\delta\chi_j,\delta\dot{\chi}_j\}$ components,

$$\delta\ddot{\chi}_j=J_x\Delta\,\delta\chi_j+\epsilon_x\Delta\,\delta\dot{\chi}_j, \quad (16)$$

where Δ denotes the discrete Laplacian. Fourier transformation gives

$$\delta\ddot{\chi}^q(t)=-4J_x\sin^2\left(\frac{q}{2}\right)\delta\chi^q(t)-4\epsilon_x\sin^2\left(\frac{q}{2}\right)\delta\dot{\chi}^q(t) \quad (17)$$

so that each Fourier component $\delta\chi^q$ is a linear damped oscillator (with damping coefficient dependent on wave number q), and we conclude that *no extended instabilities in the χ components can occur*.

Regarding the linearized equations for the $\{\delta\phi_j,\delta\dot{\phi}_j\}$ components,

$$\delta\ddot{\phi}_j=J_x\Delta\,\delta\phi_j+\epsilon_x\Delta\,\delta\dot{\phi}_j-2J_y\cos(2\phi_\infty(t))\,\delta\phi_j-2\epsilon_y\delta\dot{\phi}_j \quad (18)$$

one can proceed in the following way: First, a transformation similar to (9), that is $\delta\phi_j = \exp(\epsilon_y t)\gamma_j$, followed by the Fourier transformation $\gamma_j = \exp(iqj)\gamma^q$, lead to a damped Hill equation,

$$\ddot{\gamma}^q + [E(q) + f(t)]\gamma^q + 4\epsilon_x \sin^2\left(\frac{q}{2}\right)\dot{\gamma}^q = 0, \tag{19}$$

where $E(q) = 4(J_x - \epsilon_x\epsilon_y)\sin^2(q/2) - \epsilon_y^2$ and $f(t) = 2J_y \cos(2\phi_\infty(t))$.

Now, if $\tilde{E}(q) = E(q) - 4\epsilon_x^2 \sin^4(q/2)$, the final transformation $\gamma^q = \exp((-2\epsilon_x \sin^2(q/2))t)\,\nu^q$ leads to a Hamiltonian Hill equation,

$$\ddot{\nu}^q + [\tilde{E}(q) + f(t)]\nu^q = 0 \tag{20}$$

for the transformed variables ν^q, which are related to the initial $\delta\phi_j$ through

$$\delta\phi_j(t) = e^{iqj} e^{-(\epsilon_y + 2\epsilon_x \sin^2(q/2))t} \nu^q(t). \tag{21}$$

Denoting by $\rho_q^{\max}$ the maximum of the two characteristic exponents of the Hill equation (20), one obtains the following condition:

$$\rho_q^{\max} < \epsilon_y + 2\epsilon_x \sin^2\left(\frac{q}{2}\right) \quad \text{for all } q \tag{22}$$

for the stability of the homogeneous solution of the ladder.

C. Tail analysis

In the forced and damped systems of nonlinear oscillators that we are analyzing, the ''background'' uniform state, which is approached by the DB solution far from its localization center, $\{u_\infty(t)\}$ (FK model) or $\{0, \phi_\infty(t)\}$ (Josephson ladder), is not a rest state, but a uniform oscillation. In this section, we will assume that these oscillations have a very small amplitude, so that we can discard in the linearized Eqs. (4) and (7) terms of orders higher than linear in $u_\infty(t)$ and $\phi_\infty(t)$, respectively. This amounts to neglect, for the localization center, for the time dependence of the corresponding coefficient in the linearized Eqs. (4) and (7). This approximation, which is valid for not too large values of the parameter F_{ac}, simplifies matters for we are left with the standard problem of a linear chain with damping, which can be exactly solved (see also Ref. 19).

We consider first the linearized equations (4) of motion around the DB in the Frenkel–Kontorova model. Under the previous assumption, for $|j| \gg 1$ the coefficient $\cos(2\pi u_j(t))$ is thus set to unity, if one discards terms less than or equal to $u_\infty^2(t)$. Now we consider a semi-infinite chain with the boundary condition at the edge given by $\epsilon_0(t) = \exp(-i\omega t)$, and look for solutions of (4) of the form

$$\epsilon_j(t) = e^{(-\xi + iq)j} e^{-i\omega t}. \tag{23}$$

After insertion of (23) into Eq. (4) one obtains for the real and imaginary part, respectively,

$$\cosh\xi \cos q = 1 + \frac{1}{2C}(1 - \omega^2), \tag{24}$$

$$\sinh\xi \sin q = \frac{\alpha\omega}{2C}. \tag{25}$$

These algebraic nonlinear equations have to be solved for $q(\omega)$ and $\xi(\omega)$ assuming fixed values of dissipation α and coupling C. The familiar dispersion relation for the extended normal mode solutions (phonon band) of the discrete Hamiltonian lattice,

$$\omega^2 = 1 + 4C \sin^2(q/2), \tag{26}$$

$$\xi = 0, \tag{27}$$

along with nonzero inverse decay length $\xi(\omega)$ given by

$$\omega^2 = 1 - 4C \sinh^2(\xi/2), \tag{28}$$

$$\omega^2 = 1 + 4C \cosh^2(\xi/2), \tag{29}$$

for values of ω, respectively, below and above the phonon band, are obtained in the Hamiltonian ($\alpha = 0$) case. Only small oscillations with frequency in the band, i.e., $\omega \in [1, 1 + 4C]$, are extended ($\xi = 0$). Small oscillations with frequency outside the phonon band are damped out far from the edge of the semi-infinite chain, that is to say, they are exponentially localized. This serves to illustrate how the Hamiltonian breather needs to have all breather harmonics $n\omega_b$ out of the phonon band, so that the small oscillations associated to these frequencies decay exponentially with the characteristic length $\xi^{-1}(n\omega_b)$, and the size of the Hamiltonian breather is $\xi_b^{-1} = \sup_n \xi^{-1}(n\omega_b)$.

When $\alpha \neq 0$, we have that $\xi(\omega) \neq 0$. Thus, any solution decays exponentially. An example of the solutions $\xi(\omega)$ and $q(\omega)$ of Eqs. (24) and (25), for the particular values $\alpha = 0.02$ and $C = 0.75$, appears in Fig. 2. For purposes of comparison, the graphs corresponding to the same value of coupling for the Hamiltonian case are included.

Note that for the existence of damped-forced discrete breathers there is no need of a nonresonance condition (in contrast with the Hamiltonian case), because for any frequency ω, $\xi(\omega) \neq 0$. However, for low values of α, if some breather harmonic $n\omega_b$ belongs to the interval of values of ω for which $\xi(\omega)$ is very small, the breather profile will show large ''wings.''

For the Josephson ladder, under the assumption that $\cos(2\phi_\infty(t)) \simeq 1$, the tail analysis leads to

$$\omega^2 - (2\epsilon_x \sinh\xi \sin q)\omega + 2J_x \cosh\xi \cos q - 2J_x - 2J_y = 0, \tag{30}$$

$$(2\epsilon_x \cosh\xi \cos q - 2\epsilon_x - 2\epsilon_y)\omega + 2J_x \sinh\xi \sin q = 0. \tag{31}$$

The dispersion relation for the Hamiltonian ladder is

$$\omega^2 = 2J_y + 2J_x(1 - \cos q) \tag{32}$$

and the phonon band is restricted to

$$\omega_{\min} = \sqrt{2J_y} \leqslant \omega \leqslant \sqrt{4J_x + 2J_y} = \omega_{\max}. \tag{33}$$

Outside this phonon band, ξ is equal to

$$\xi = \cosh^{-1}\frac{2(J_x + J_y) - \omega^2}{2J_x} \quad \text{if } \omega \leqslant \omega_{\min}, \tag{34}$$

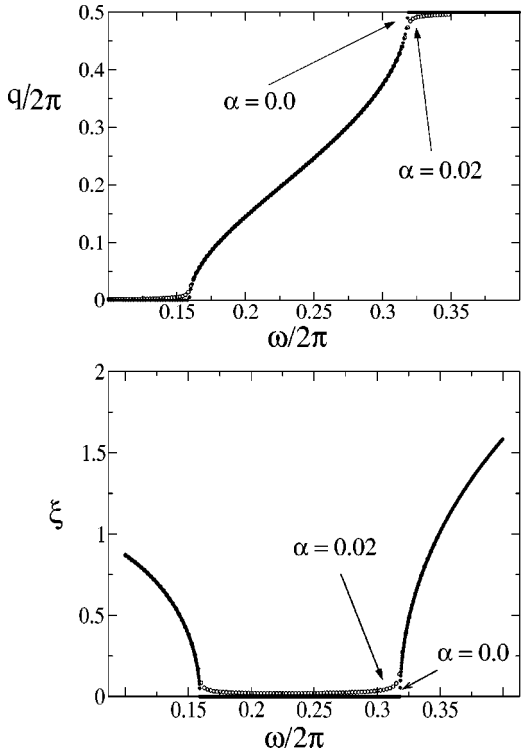

FIG. 2. Tail analysis of dissipative DB's in the Frenkel–Kontorova model. Wave vector q and inverse of the decay length ξ as functions of ω for two different values of the damping, $\alpha=0.02$ (open circles) and the Hamiltonian case $\alpha=0.0$ (filled ones). The coupling parameter C is in both cases equal to 0.75.

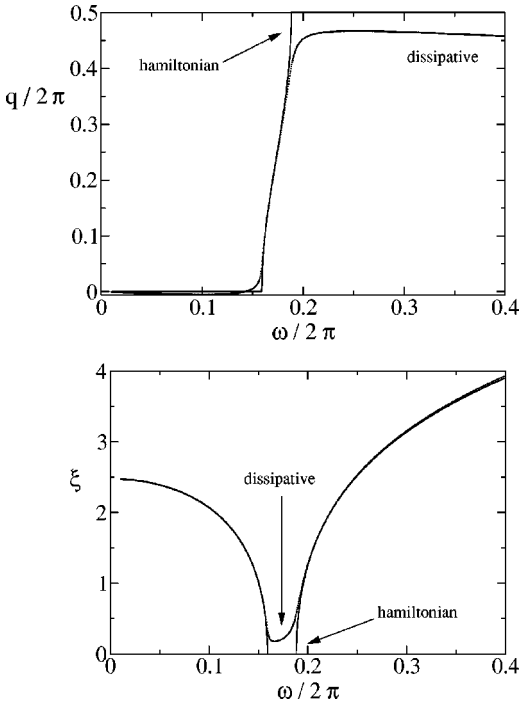

FIG. 3. Tail analysis for a rotobreather in a Josephson junction ladder. Wave vector q and inverse decay length ξ as functions of ω for the ladder parameters ($J_y=0.5$, $J_x=0.1$, $\epsilon_x=\epsilon_y=0.01$). For the latter, and outside the ''phonon band,'' the Hamiltonian and dissipative solutions almost overlap in spite of the differences between both cases shown in the q variable.

$$\xi=\cosh^{-1}\frac{-2(J_x+J_y)+\omega^2}{2J_x} \quad \text{if} \quad \omega\geqslant\omega_{\min}. \tag{35}$$

An example of the solutions $\xi(\omega)$ and $q(\omega)$ of Eqs. (30) and (31) for the values $J_y=0.5, J_x=0.1, \epsilon_x=\epsilon_y=0.01$ appears in Fig. 3 where the Hamiltonian ($\epsilon_x=\epsilon_y=0$) results are also shown. Comparing it to Fig. 2 for the Frenkel–Kontorova model, one can realize how the ''Laplacian damping'' has a strong qualitative effect on the graph of $q(\omega)$ for high values of ω.

As shown in the upper panel, for frequencies above the normal mode ones, it is not possible to reach the wave vector $q=\pi$ when the system is dissipative. That means that no ''antiferro-like'' linear mode is allowed for this system. Also for low ω there are two values with $q=0$ (or ''ferro-like'' mode in this language): the first is trivial, $\omega=0$, and the second one is $\omega=\sqrt{2J_y-2J_x\epsilon_y/\epsilon_x}$.

IV. BIFURCATIONS

In this section we will review the rich phase diagram of pinned (nonmobile) dissipative DB's in the two models under scrutiny: oscillobreather solutions in the Frenkel–Kontorova model, and rotobreathers in the Josephson junction ladder. To face this task we adopt the well-known method of continuation from the anticontinuous limit. As already mentioned in previous sections, a dissipative system has some advantages over a Hamiltonian one when it comes to finding good numerical solutions of the equations of motion. Methods in Hamiltonian systems are based on Newton (or shooting) schemes to solve the equations of the stroboscopic maps. This requires a careful computation of the equations of motion in both nonlinear and linear approximation, besides some tricks to avoid time and energy translation degeneracies. However, in dissipative systems, breathers are real attractors of the dynamics and we can forget most of the cautions one has to take in the Hamiltonian case.

Several auxiliary quantities have been computed in order to characterize completely the solutions:

(i) For periodic DB, the spectrum of Floquet multipliers was numerically computed for each solution, thus monitoring their evolution on the complex plane. This allows us to follow the linear stability of periodic attractors, locate the bifurcation points where straightforward continuation stops, and characterize adequately the type of bifurcations.

(ii) Poincaré (stroboscopic) sections of the numerical solutions. This is particularly convenient when dealing with nonperiodic DB's which (as will be seen below) often emanate from some bifurcations found in the continuation path.

(iii) The power spectrum of quasiperiodic and chaotic solutions. This is defined by

$$S(\omega)=\left|\int_{-\infty}^{\infty}\dot{x}_j(t)e^{i\omega t}dt\right|^2, \tag{36}$$

where $\dot{x}_j(t)$ denotes either $\dot{u}_j(t)$ or $\dot{\phi}_j(t)$, depending of the model under consideration. Note that we use velocities in-

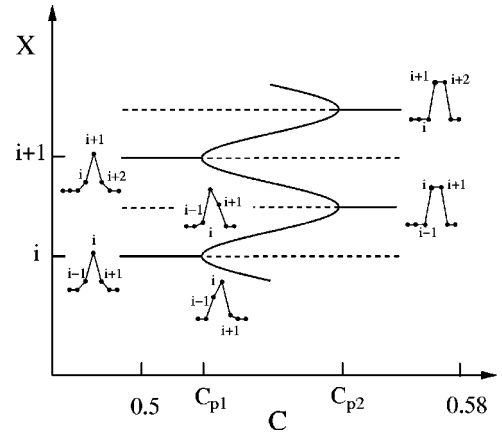

FIG. 4. Scheme showing the pitchfork bifurcations (mirror symmetry breaking transition) of the pinned periodic discrete breathers in the FK model when the coupling parameter (C) increases. The asymmetry character is measured by X (see text). Solid (dashed) lines mean stable (unstable) solutions.

stead of angles or positions for computational convenience, in particular when rotations of some variable occur, as in Sec. IV B.

A. Oscillobreathers in the FK model

We summarize here the numerical findings reported in Ref. 20 on the evolution of the properties of continued DB's when the coupling parameter is adiabatically increased from $C=0$. Let us note that both the 1-site and the 2-sites periodic continued DB's are mirror-symmetric around the localization site and bond, respectively. Both were found to be continuable until very high values of C, where the continuum limit is approached. However along the continuation path we have found many bifurcation (or branching) points where several branches of qualitatively different breather solutions meet. The bifurcations observed are of two general classes, namely *pitchfork* and *Naimark–Sacker* bifurcations.

1. Pitchfork bifurcations

At one side of the bifurcation point, a branch of mirror-symmetric stable periodic DB exists, while at the other side two stable branches of periodic mirror-asymmetric DB's and an unstable branch of periodic symmetric DB's meet. The Floquet spectrum of the stable symmetric DB shows that an eigenvalue approaches $+1$ at the bifurcation point, exiting the unit circle past the bifurcation on the unstable DB branch. The eigenvector associated to this instability is antisymmetric and exponentially localized. The two stable branches correspond to two asymmetric DB's, one being the mirror image of the other. These pitchfork bifurcations are thus (mirror-) symmetry-breaking transitions of the periodic DB's.

Figure 4 shows the branching (or bifurcation) diagram for $0.5<C<0.6$ at fixed values of the rest of parameters. In this range of C values, two pitchfork bifurcations occur at $C_{P1}\simeq 0.52962$ and $C_{P2}\simeq 0.55315$ Note that for $C<C_{P1}$ the 1-site DB is stable while the 2-sites is unstable, and that for $C>C_{P2}$ the situation has been reverted. For $C_{P1}<C<C_{P2}$, the broken symmetry DB's form the stable branches, and the symmetric branches are linearly unstable.

The breaking of the left-right symmetry renders meaningful the concept of *center X* of the breather as a continuous variable. This concept, certainly alien to the ancestral anticontinuous origin of the (1-site and 2-sites) continued DB's, serves to measure quantitatively the degree of asymmetry of the solutions on the asymmetric stable branches. The variable X is like a sort of ''order parameter'' associated with the symmetry-breaking transitions at C_{P1} and C_{P2}, or better said, is a *collective variable*, i.e., the average value (over components) of some function f on the solution, measuring its asymmetry. This value can be chosen to be the integer for the 1-site DB (now better called *site-centered* DB) and half-integer for the 2-sites DB (or *bond-centered* DB). This measure X of the asymmetry is then naturally interpreted as the center of the static breather. Collective variables of this type are commonly used to describe mobile localized excitations[21,22] though here X is purely motivated by symmetry considerations.

The connection of the pitchfork bifurcations like C_{P1} and C_{P2} to the issue of breather mobility is not limited to the emergence of the collective variable X as important breather descriptor. It turns out that the Floquet mode driving the bifurcation (symmetry-breaking mode), when added as a perturbation (of large enough amplitude) to the static stable DB's drives easily the system towards stable attaccting mobile breathers. This procedure to obtain numerical approximations to mobile breathers by perturbing static ones with antisymmetric modes was used in Hamiltonian models supporting DB's.[23,24] The term *depinning mode* was then coined to name these modes, but *symmetry-breaking* modes is an equally correct term, as mobility requires (at some level) the breaking of the left–right symmetry by the mobile solution.

Pairs of pitchfork bifurcations with a branching diagram as shown in Fig. 4, occurs repeatedly when C increases, as a ''broadening mechanism'' by which the DB's width growths. The Floquet eigenvalue associated to the symmetry-breaking bifurcations remains closer and closer to $+1$ at all times, announcing the appearance of a Goldstone mode (due to continuous translational invariance) as $C\to\infty$. This was ostensibly manifest at $C\gtrsim 5$.

2. Naimark–Sacker bifurcations

Also known as *generalized Hopf bifurcations* or *Hopf bifurcations of periodic solutions*. At the bifurcation point, two complex conjugate Floquet multipliers of the periodic continued DB cross the unit circle at $\exp(\pm i\varphi)$, with $\varphi\neq 0$, and the periodic breather becomes unstable. In the simplest case, called supercritical, a two-frequency (ω_b and $\varphi\omega_b/2\pi$) stable quasiperiodic DB borns out of the bifurcation. In the subcritical case, an unstable quasiperiodic attractor merges with the stable periodic DB. We have observed both subcritical and supercritical Naimark–Sacker bifurcations.

Figure 5 shows an example of a stable 2-site quasiperiodic DB. The power spectrum for one of the particles in the breather core shows peaks at linear integer combinations of two basic frequencies. Though the lack of periodicity of these solutions prevents the use of Floquet analysis to study

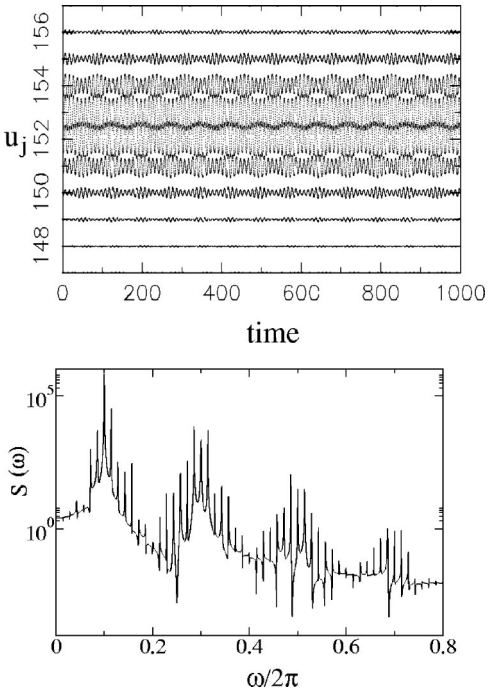

FIG. 5. Two-site quasiperiodic oscillobreather in the Frenkel–Kontorova model. Note that particles on both sides of the breather are out of phase. The figure below shows the power spectrum of one of the central particles. The peaks are linear combinations of the two frequencies.

their stability, the attracting character of this quasiperiodic DB can be numerically ascertained, checking its robustness against small perturbations. We have to emphasize here the strong sense of stability that these quasiperiodic solutions satisfy: They are attractors of the dynamics, possessing an open set (basin of attraction) of initial conditions asymptotically converging to the DB. The inspection of figure reveals that an adequate description of this DB in terms of the collective variable X is that of a breather oscillating in a (Peierls–Nabarro-type) potential well. From this perspective, the Neimark–Sacker bifurcation would be an instability of the ''constant X'' pinned breather, leading to an ''oscillating X'' pinned breather. Another suggestive description of this quasiperiodic DB is to look at it as a ''beating solution'' for the two central oscillations.

The example shown in figure belongs to a stable branch of quasiperiodic DB. This branch has an interval of instability ($0.88<C<0.96$) where the breather spontaneously moves. No pinned (periodic or quasiperiodic) stable DB exists in that parameter interval: Only mobile breathers occur for that (relatively narrow) range of coupling. These mobile breathers are not continuation of the mobile breathers induced by perturbing static DB's with symmetry-breaking modes, but seem to born out straight from the destabilization of quasiperiodic pinned DB. No stable pinned breather coexists anymore within this interval with mobile attracting breathers.

B. Rotobreathers in the Josephson ladder

Here we summarize the main features of the phase diagram of rotobreather solutions in the anisotropic Josephson junction ladder previously studied in Ref. 25. As in the Frenkel–Kontorova model analyzed in the previous subsection, we have found several different bifurcations. Moreover, due to the existence of more tunable parameters and the fact that we have now two variables (ϕ,χ) per site, the complexity of different scenarios is correspondingly greater than for the Frenkel–Kontorova model. In what follows we describe some of them. First, we must remark that the tool used for describing the nature of the bifurcations is Floquet analysis (see Sec. III A) and therefore we are restricted to periodic rotobreathers. Moreover, along this section the initial rotobreather we use is uniformly zero in χ variables (see Sec. II B) and exponentially localized in ϕ's.

As it is a nonexhaustive exploration we keep fixed some of the parameters ($J_y=0.5$, $\epsilon_y=0.01$, $\omega=1.5$) while varying the others (J_x, ϵ_x, I_{ac}). Prior to the detailed description of each observed bifurcation we summarize them in Fig. 6.

The first observed bifurcation was found when the Josephson horizontal coupling (J_x) increases above values around $J_x\sim 0.105$. The associated Floquet multiplier leaves the unit circle at -1 and the corresponding eigenvector has zero components along $\delta\phi_i$ and $\delta\dot{\phi}_i$ and nonzero along $\delta\chi_i$ and $\delta\dot{\chi}_i$. This destabilizing mode is exponentially localized around the center of the rotobreather solution (the study done in Sec. III B shows that no extended instabilities can occur in the initially uniform χ components of the breather). The absence of an on-site pinning potential term in the equations of motion (3) makes the new localization length scale in the χ variables much larger than in the ϕ ones. Other characteristics of the new oscillo χ-breather are spatial symmetry, an almost ''antiferro-like'' profile and a time period twice the period of the (ϕ) rotobreather. This instability is almost insensitive to changes in the parameters I_{ac} and ϵ_x (see panel a in Fig. 6). Extending the study but now to the new combined ϕ-χ-breather arising from the bifurcation shows that it only survives a small increase in J_x before it becomes unstable and disappears.

A second type of instability occurs when the current intensity I_{ac} is increased, while keeping fixed J_x and ϵ_x. Here the Floquet multiplier that drives the instability process leaves the unit circle through -1. The associated eigenvector has zero components along $\delta\chi$ and $\delta\dot{\chi}_i$ and nonzero in the ϕ's. Again, as in the previous case, the profile of the eigenvector is localized around the breather center. The new rotobreather obtained after perturbing the initial one along the eigenvector direction has twice the period than the one before the bifurcation, so the instability is a typical period-doubling bifurcation. Beyond the first one either further period doubling processes occur or an inverse period doubling can appear sometimes to bring the rotobreather solution back to the previous period.

A third type of bifurcation destabilizing the rotobreather is generally found when the parameter ϵ_x is increased. Here the Floquet multiplier leaves the unit circle at $+1$. The associated eigenvector is also localized in ϕ's and null in χ's with a localization width of the order of that of the initial rotobreather. Perturbing along the eigenvector brings it into the basin of attraction of the uniformly oscillating solution. It is likely a saddle-node bifurcation. The ϵ_x value at which the

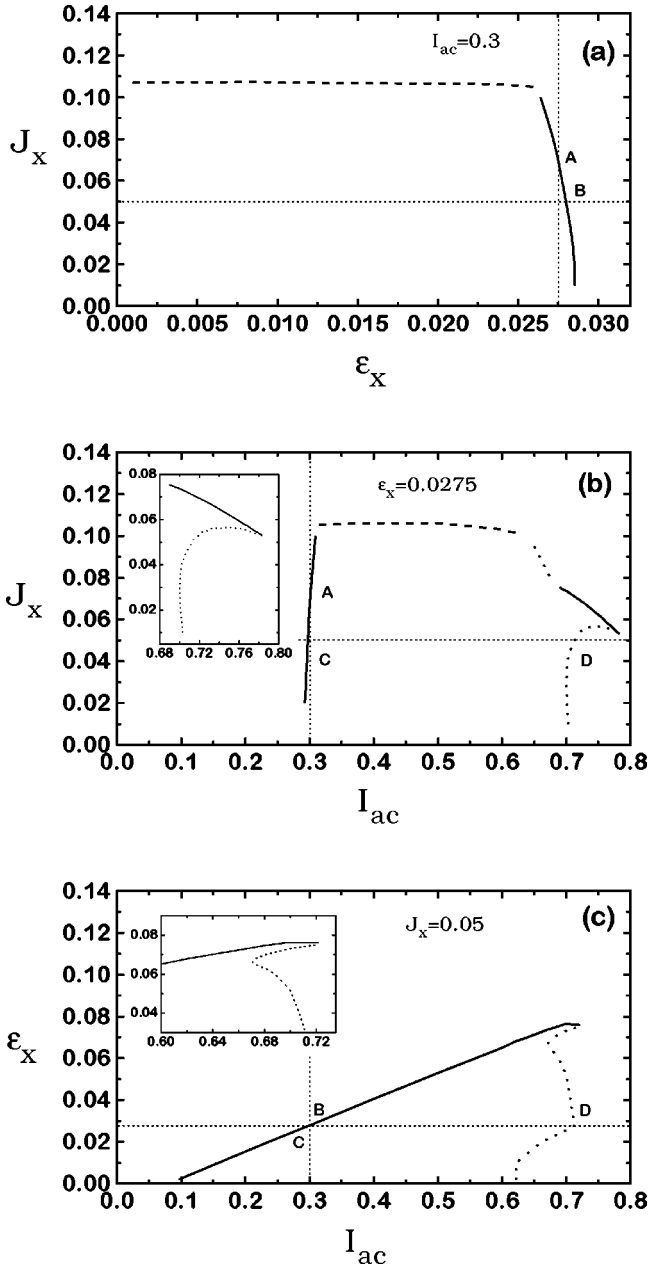

FIG. 6. Two-dimensional sections of the three-dimensional (J_x, ϵ_x, I_{ac}) explored parameter space of the JJ ladder. The different lines are the frontiers where a given instability is observed in the Floquet analysis of the periodic rotobreather. Widely dotted lines correspond to period doubling bifurcations (only the first one is shown for the sake of clarity, but a second, third, etc., can occur). Broken lines represent χ-instability bifurcations, and continuous lines indicate saddle-node bifurcations. Tightly-dotted straight lines in each plane are the corresponding intersections with the other planes. The points *A*, *B*, *C*, and *D* are indicated to ease 3*D* mental reconstruction.

bifurcation occurs increases with increasing current intensity I_{ac} [see panel (c) in Fig. 6], a fact which agrees with the simple physical intuition that the effects of both parameters on the central rotating $\phi_j(t)$ oppose each other.

We have shown here how the many parameters of the model besides the two variables per site increase the complexity of possible bifurcations. We could also make variations in the other three parameters kept fixed in this work and other possible scenarios could arise. Actually, in the next section we analyze another interesting case when the parameter that we change adiabatically is ω.

C. Chaobreathers

One of the more interesting features found in the bifurcation analysis of rotobreathers in the anisotropic Josephson junction ladder biased by external currents, was the existence of chaotic rotobreather solutions,[26] where the ''degree'' of chaoticity is also exponentially localized in space (Fig. 7).

The discovery was made when varying ω continuously and keeping fixed $J_x=0.05$, $J_y=0.5$, $\epsilon_x=0.03$, $\epsilon_y=0.01$, $I_{ac}=0.72$. Around the value $\omega=1.623$ a subharmonic cascade of period doubling bifurcations transforms the initial exponentially localized periodic rotobreather into an also exponentially localized but chaotic rotobreather. This case looks like the period doubling bifurcations observed when the external current is increased (see previous subsection) but in that case a complete subharmonic cascade was never detected.

To analyze the chaotic character of the rotobreather solution one can compute numerically the spectrum of Lyapunov exponents and obtain the Lyapunov dimension.

Arguments about the genericity of the existence of chaotic breathers in other nonlinear systems were given in Ref. 26 and also numerically confirmed in a chain of harmonically coupled and forced van der Pol oscillators,

$$\ddot{\phi}_i = -\mu(\phi_i^2-1)\dot{\phi}_i - \phi_i + b\cos\omega t + C(\phi_{i+1}-2\phi_i+\phi_{i-1}). \tag{37}$$

It was easy to find in the literature[27] the parameter region where three different attractors coexist for the single forced and damped van der Pol oscillator, two of them chaotic and the other periodic. The continuation method allowed us to follow the evolution of a chaotic breather-like uncoupled solution (the central oscillator in one of the strange attractors and the rest of the chain in the periodic one) up to coupling strengths significantly different from zero while preserving the chaotic nature. Another example of chaotic rotobreathers is reported in Ref. 28, where a 1*D* driven damped lattice of dipoles was studied.

Although this numerical evidence provides strong support for the existence of chaotic DB in generic forced and damped lattices of nonlinear oscillators, a rigorous proof of existence has been sketched[29] only under strong mathematical conditions (uniform hyperbolicity), which usually are not satisfied in realistic physical models.

Chaotic mobile DB have been observed numerically as long-lived transients in Hamiltonian systems, but exact Hamiltonian chaotic DB could not exist, due to the ''broad band'' structure of the power spectrum of chaotic trajectories, which would violate the nonresonance condition.

V. MOBILE AND INTERACTING BREATHERS

A. General remarks

In the previous section we have shown how diverse new properties (e.g., mirror asymmetry, quasiperiodicity, chaos) appear as characteristics of some branches of attracting discrete breathers that emerge from the diverse bifurcations one

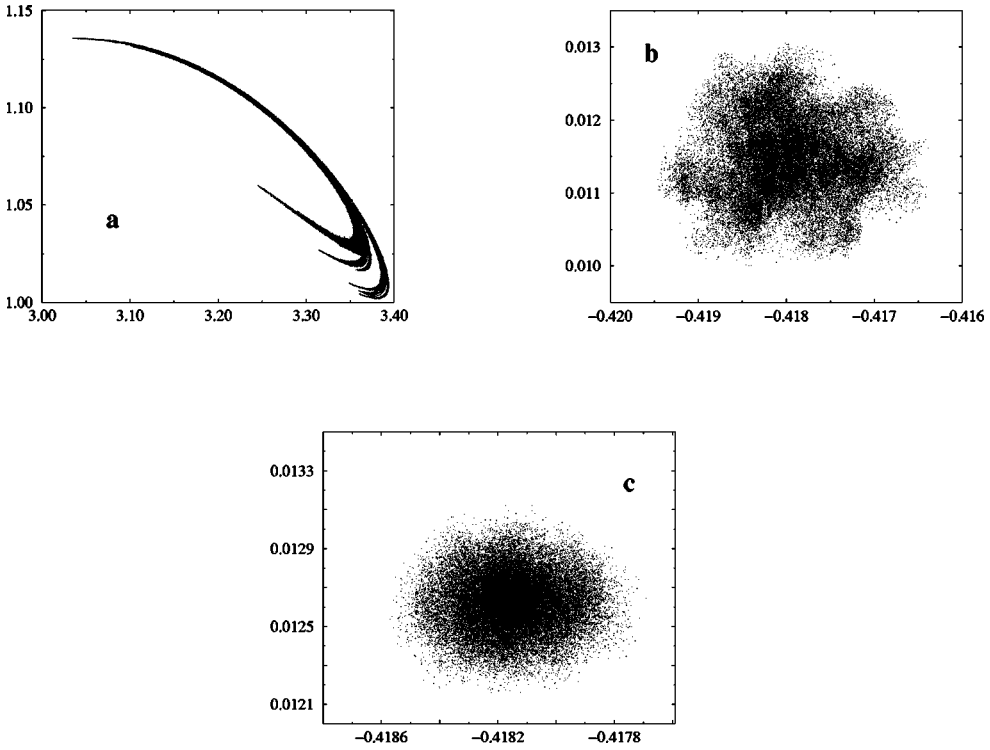

FIG. 7. Poincaré sections of the trajectories $\phi_i(t)$ at times $t+n2T_b$, for three different oscillators of the chaobreather in the JJ ladder. The pictures show the planes $\dot{\phi}$ (in radians per unit time) versus ϕ (in radians) for the rotor (a), its fifth neighbor (b) and the ninth one (c). Notice the very different scales of (b) and (c) in order to see the spatial localization of the chaotic contribution to the dynamics of each oscillator.

finds along the continuation path numerically followed. Another property of some attracting branches of breather solutions is *mobility*. We have already remarked (from pure symmetry considerations) the convenience, as quantitative descriptor of the breather, of using a collective variable X real and continuous, which is naturally interpreted as center of the localization of energy. Mobile breathers are solutions where the average value of the breather center X unboundedly increases (or decreases) as time goes by.

Observations of *moving* breather-like excitations have been made both in Hamiltonian[23,24] and dissipative systems.[20] Contrary to the case of pinned breathers, there is, at present, no exact proof of existence for mobile breathers (MBs), i.e., breathers exhibiting translatory motion. However, the observed excitations appear to be quite stable in simulations, and in the case of the dissipative and driven Frenkel–Kontorova model (1) numerically have been found to be attractors of the dynamics.[20] The most typical type of pinned breather is a periodic solution of the equations of motion. For a MB with a translation velocity $v_b \neq 0$, *strict* periodicity is possible if the system itself is a ring of size L and the time $T=L/v_b$ required by the breather to travel round the ring once is related to its internal period $T_b = 2\pi/\omega_b$ by $mT=nT_b$, where m,n are integers (another possibility would be that the breather is reflected twice from the opposite ends of a finite chain, and the above considerations can be reinterpreted accordingly). As often one prefers to think of the system as an infinite chain rather than a finite size ring and because requirements on the system's size like that above may be considered as too restrictive, periodicity can be taken as periodicity up to integer position shifts (we consider a lattice of periodicity 1). This requires $v_bT_b = m/n$, with m,n as integers.[30] In the following we will not restrict our discussion to such "periodic" solutions and consider a MB to be a solution with an internal degree of freedom (oscillation or rotation) that propagates along the system.[21] The internal degree of freedom need not be periodic, but can have a spectrum of incommensurate frequencies.

The oscillations of the internal degree of freedom can generate phonons in the system. As for the relation between the frequencies of the phonons and the frequency or frequencies of the breather, it has to be taken into account that a (angular) frequency ω_0 in the restframe of the MB is Doppler-shifted due to the translatory motion of the breather, according to

$$\omega(q)=\omega_0+v_bq. \tag{38}$$

Here q is the wave vector in the restframe of the chain, and ω is the frequency observed in this frame. Depending on the complexity of the dispersion relation $\omega(q)$, a numerical solution of (38) can be called for. Note that every ω_0 leads to two frequencies $\omega(q_1)$ and $\omega(q_2)$, one for emission in the direction of the propagation, one for the opposite direction; for higher dimensional systems things can be more complicated, as there are infinitely many intermediate directions. Another point to be taken into account is that the propagation at velocity v_b of the MB along a system of periodicity 1 (the rescaled lattice constant) constitutes a perturbation of frequency $2\pi v_b$ as seen in the MB restframe. Due to the nonlinearity of the system, combination frequencies $m\omega_b + n2\pi v_b$, m,n integer, can be created, which then are also Doppler-shifted. Many phenomena of the dynamics of solitary waves successfully have been described within a collective variable approach, e.g., Refs. 22, 31, and 32. This approximation aims at capturing the main features of the dynamics of a large (or infinite) number of degrees of freedom, those of the constituents of the system, by the dynam-

ics of considerably fewer variables that are appropriate for a collective description of the solitary excitation. The most important example of a collective variable is the position of a solitary wave, other examples can for instance be found in Ref. 33. There exist different ways of introducing collective variables, but typically integrations over functions that describe the shape of a solitary wave are involved. As this shape does not explicitly depend on time, but only on the collective variables, one eventually arrives at equations for the collective variables where all reference to the time dependence of the constituents of the system has disappeared. Thus only the collective variables remain as dynamical quantities; this usually is a great simplification. For breathers, on the other hand, the explicit time dependence of the shape is a distinguishing feature and a standard collective variable treatment is problematic: The collective variable equations explicitly contain time. This time dependence stems from the constituents of the system and requires that the time dependence of the breather solution is known. So, usually, a real simplification is not possible. Recently, a different type of collective variable technique has been presented for breathers in Hamiltonian systems:[21] Breather solutions are considered as loops in phase space. The loops are characterized by a set of parameters μ that play the role of collective variables. The dynamics in phase space is tranferred to a dynamics in the space of loops by averaging over one period of a loop. As an approximation, the dynamics in loop space is considered to be sufficiently well described by the time evolution of the parameters μ. The last step corresponds to the reduction of the dynamics of a solitary wave bearing system to the dynamics of the collective variables describing the solitary wave.

B. Peierls–Nabarro barrier

The notion of the Peierls–Nabarro barrier of a localized excitation arises naturally when mobile localized excitations are studied in *discrete* systems. It is associated with the lack of continuous translational invariance, the symmetry group of translations being discrete. If we consider a solitary excitation, the part of the energy not associated with kinetic energy of translation can depend on the position X of the solitary excitation. Recording this part of the energy as a function of X while moving the excitation from one lattice site to the next usually results in a nonconstant graph. The difference between the maximum and the minimum of this curve can be considered as the Peierls–Nabarro barrier, i.e., the minimum energy necessary for shifting the excitation from one site to the next. If the total energy of the excitation is below this barrier, i.e., if the kinetic energy is too small, then the excitation is trapped at one site and cannot travel through the system. The height (and shape) of the barrier depends on the shape of the solitary wave. In the case of a breather, this shape is subject to (quasi)periodic oscillations, so the energy barrier the breather has to cross in order to get from one lattice site to the next depends on the internal degrees of freedom of the breather. A more elaborate discussion can be found in Ref. 34. Whereas it is therefore not possible to define a Peierls–Nabarro potential for breathers in a way completely analogous to the definition of this potential in the case of ''simple'' (i.e., without additional internal degrees of freedom) solitary waves, related quantities can be introduced, for example, a depinning energy. The Floquet-matrix of certain breathers possesses localized eigenvectors $\{\boldsymbol{\epsilon}_n(t)\}$ corresponding to spatially antisymmetric internal modes. These modes have been used to turn a pinned breather into a mobile one. Following Ref. 24 the optimal way to do this uses only the velocity parts of this mode: If $\{u_n(t)\}$ denotes the breather configuration, the perturbed initial configuration is obtained as

$$u_n^{\mathrm{per}}(t=0,\lambda)=u_n(0), \quad \dot{u}_n^{\mathrm{per}}(t=0,\lambda)=\dot{u}_n(0)+\lambda\,\dot{\boldsymbol{\epsilon}}_n(0). \tag{39}$$

Note that in this case, by the choice of $t=0$, the internal degrees of freedom are fixed to a certain ''phase'' at the instant of the perturbation. A minimal magnitude λ_c of the perturbation is necessary in order to initiate translatory motion of a breather. The velocity of the thus generated MB depends on $\lambda-\lambda_c$ for the Hamiltonian system. It has been proposed[23] to use the threshold λ_c as a means to define a Peierls–Nabarro potential barrier for moving discrete breathers. If, in (39), $\{u_n(0)\}$ is chosen as a breather configuration at an instant of its internal motion where all particle velocities $\dot{u}_n=0$, and if the vector $(\mathbf{0},\dot{\boldsymbol{\epsilon}}(0))$, the $\mathbf{0}$ representing the vanishing elongation part of the perturbing vector, is normalized, then indeed the energy of the perturbation is $\frac{1}{2}\lambda^2$, and correspondingly $\frac{1}{2}\lambda_c^2$ can be interpreted as an energy barrier to be overcome in order to excite a nonzero translation velocity of the breather and therefore as a depinning energy.

A different way of introducing the concept of a Peierls–Nabarro potential can be found in Ref. 31. There, as mentioned in the previous section, the dynamics is described as dynamics in a space of loops, where the internal degrees of freedom are averaged out. At the level of the averaged dynamics, a Peierls–Nabarro potential can be introduced in a well-defined way. The interested reader will find in Ref. 35 a tutorial introduction to these ideas for Hamiltonian systems.

Our focus here is on forced-damped discrete breathers and it is important to realize the formal and conceptual differences this makes regarding the notions of the Peierls potential and depinning energy. In a periodic solution, an exact balance of input power (by the external forcing) and dissipated power is kept over a period of time t_b, and instead of energy conservation, only power balance holds. Moreover, the stroboscopic section of the phase space is partitioned in basins of attraction, and the structure of basin boundaries, can be seen as a net of barriers to dynamics. Pinned periodic discrete breathers are fixed points of the stroboscopic map, while the sections of attractor mobile breather trajectories are (generally) expected to fill a continuous line for noncommensurate velocities.

A simple scenario, that occurs for the forced and damped FK model in some ranges of couplings, is sketched in Fig. 8. There, a sequence of alternating attractor-saddle (stable-unstable) pinned breathers located at positions $\ldots,X_1,X_1^*,X_2,X_2^*,\ldots$ coexist with a stable attracting $\tilde{X}(t)$ mobile discrete breather solution. Certain directions $\{\boldsymbol{\epsilon}_n,\dot{\boldsymbol{\epsilon}}_n\}=|\boldsymbol{\epsilon}\rangle$ in the tangent space of an attracting pinned

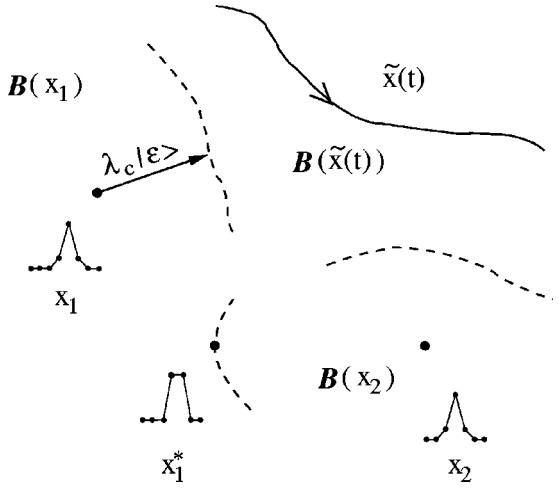

FIG. 8. Simple scheme of alternating stable–unstable pinned breathers with their basins of attraction (whose boundaries are dashed lines), coexisting with a mobile breather solution (solid line). A perturbation strong enough along the $|\epsilon\rangle$ direction is able to move the breather located at X_1 into the basin of attraction of the mobile discrete breather.

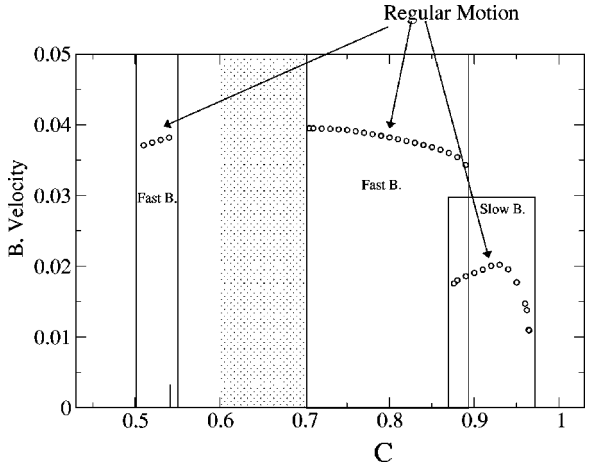

FIG. 9. Single-breather velocity as a function of the coupling C, in the Frenkel–Kontorova model. The values of the rest of the parameters are $\alpha=0.02$, $F_{ac}=0.02$, $\omega=0.2\pi$. In the shaded region the breathers exhibit irregular motion. This figure has been taken from Ref. 20.

solution (like X_1 in Fig. 8) bring this into the basin of attraction $\mathcal{B}(\tilde{X}(t))$ of the mobile breather $\{\tilde{X}(t)\}$, i.e., $\{X_1\}+\lambda|\epsilon\rangle \in \mathcal{B}(\tilde{X}(t))$ for some λ. Let us call $\lambda_c(|\epsilon\rangle)$ the minimal strength (in the $|\epsilon\rangle$ direction) to turn the pinned solution into mobile, and then define λ_c^* as the $\inf_\epsilon \lambda_c(|\epsilon\rangle)$. This quantity, measuring the ''shortest'' distance from the pinned breather to the basin of mobility, is the dissipative counterpart of the quantity λ_c defined in the previous paragraph, i.e., the threshold strength of a depinning perturbation. As before, it could generally depend on the choice of time (modulo t_b) of the stroboscopic section. On the other hand, if $\mathcal{E}(X_1)$ and $\mathcal{E}(X_1^*)$ denote some potential energy (not including the kinetic energy of the breather translation) associated with X_1 and X_1^* (pinned attractor and saddle, respectively) one could arguably define the Peierls–Nabarro barrier for breather shifts as $\mathcal{E}(X_1^*)-\mathcal{E}(X_1)$, but the use of it has to be connected to the power balance governing the dynamics.

Other different scenarios are possible. Notably, as described in Sec. IV A, we have observed the situation in which no stable pinned breather solutions exist, but only running stable DB solutions are found. None of the previous quantities seem to make much sense in terms of utility, in this situation when no reference stable pinned solution is available.

C. Mobile breathers in the dissipative and driven FK model

As mentioned above, in this model mobile breathers do exist as attractors of the dynamics. In Fig. 9, taken from Ref. 20, the velocity for the MBs is shown as a function of the coupling C. The other parameters have been $\alpha=0.02$, $\omega=0.2\pi$, and $F_{ac}=0.02$. There exists two types of MB that are clearly distinguishable by the range of their velocities. The faster breathers, found for $0.5<C<0.56$ and $0.7<C<0.88$ have been created by perturbing a pinned breather according to (39). These breathers are therefore called *induced fast breathers*. It is this procedure, and the eigenvector involved, that are connected to the symmetry-breaking pitchfork bifurcation at C_{P1} discussed in Sec. IV. The slower breathers, for $0.88<C<0.96$ arose in the continuation with respect to C without any additional perturbation required. They have been termed *spontaneous slow breathers*. In a narrow C-range around $C=0.89$ both types of breather coexist. Beyond $C=0.96$ the breathers are again pinned. In the region $0.6<C<0.72$ MBs exist, but their motion is irregular, with apparently random sudden changes in velocity. Boundary crisis type of bifurcations have been invoked[20] to explain this regime of erratic mobility.

The MBs have phonon tails decaying in space. A Fourier analysis of the oscillations in the tails reveals spectra that can be interpreted as Doppler-shifted combination frequencies of the driving frequency and $2\pi v_b$, as already indicated above. For the parameters used in this review[36] there is no commensurability between these frequencies, so the MB is a quasiperiodic solution. Due to the Doppler-shifts, the tails of a MB are asymmetric. The phonon tails play an important part in collisions of two breathers, as the interaction between the breathers is mediated by phonons. Numerical experiments show that there are basically four types of final states for a collision or scattering process of two MBs: the breathers can rebounce from each other, one of the breathers can be annihilated, both breathers can be destroyed, or the breathers can form a ''bound state.'' A bound state is a configuration of two breather cores situated at a certain distance from each other, propagating along the system together. Bound states of velocity zero have also been found.[20]

The simulation of scattering processes shows that at larger separation the propagation of the colliding breathers seems to be unaffected by their respective collision partner, and that there is a kind of ''effective range'' of the interaction (≈ 160) where the system selects one of the four types of final states. However, it has been found also that the final state can be changed by noise so weak that no thermal fluctuations are visible in the energy distribution of the system on a scale set by the energy peaks of the breather cores. Moreover, though the breather tails are exponentially

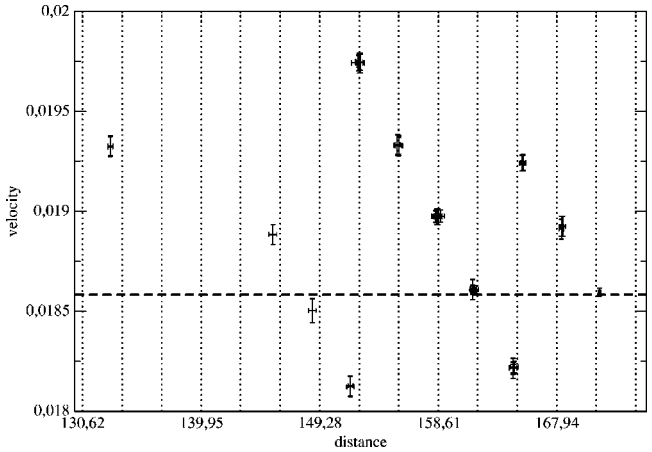

FIG. 10. Values of distance and velocity for bound states. The position of the breathers was determined every 5000 time units, up to a total of 50000 time units. This gives 10 values for the velocity and 11 (10+initial) for the distance. The average of these values enters the diagram, error bars denoting one standard deviation. The dashed line indicates the velocity of a single breather (parameters: $C=0.890$, $\alpha=0.02$, $F_{ac}=0.02$, $\omega=0.2\pi$; system size: 1000 particles). The dotted lines are spaced equidistantly.

damped, they still appear to be strong enough to influence the scattering, as changes in the boundary conditions between periodic and free can change the qualitative result of a scattering process given otherwise identical initial conditions. This we have observed for a system of 1000 particles. As shown in Fig. 9, at a given value of the system parameters, there is a unique value of the velocity of a single breather (apart from the small overlap between the induced fast breather and the spontaneous slow breather regimes). In numerical scattering experiments with spontaneous slow breathers a larger number of different bound states was found. Two of their main characteristics, the distance between the breather cores and the propagation velocity, are shown in Fig. 10. The chart contains the data from over 50 bound states. It is obvious that certain values of the distance are preferred and that moreover there is a relation between distance and velocity. Clearly, several different values of the velocity are now possible at fixed values of the system parameters. There is evidence that the phonons between the breather cores play a decisive part in the selection of ''allowed'' distance–velocity pairs. The precise mechanism leading to the results shown in Fig. 10 is under investigation.

VI. CONCLUSIONS

Numerical studies of DB's in forced and damped lattices of nonlinear oscillators (or rotors) allow a detailed investigation of the properties of these exact localized states and how they vary as different parameters of the physical models are tuned. Compared to the Hamiltonian case, numerical procedures of adiabatic continuation are here simpler, faster, and more reliable, due to the character of local attractor that these exact solutions enjoy. The robustness of these intrinsic localized states against all kinds of perturbations (including stochastic) allows us to consider dissipative discrete breathers as ''potentially observable'' states in experimental situations.

The existence of bifurcation (pitchfork, Naimark–Sacker, period doubling, etc.) in the the continuation path of DB's, where new branches of localized solutions emerge, originates DB's with new properties: mirror-symmetry breaking (i.e., asymmetric), quasiperiodic, and chaotic discrete breathers appear as attractors of the nonlinear dynamics in some ranges of the models parameters. While quasiperiodic and chaotic DB's are impossible as exact solutions in Hamiltonian systems, intrinsic localization has been shown to persist in forced-damped systems under quasiperiodic and even chaotic instabilities of the breather core.

We have motivated the use of a collective variable X (the breather position) parametrizing the branches of asymmetric DB's. This collective variable assumes a prominent role in the description of mobile localized excitations, leading to the discussion of the concepts of the Peierls–Nabarro barrier and depinning energy. Branches of attracting mobile dissipative DB's have been numerically continued in the Frenkel–Kontorova model with periodic driving and viscous damping. These mobile DB's are capable of forming two-breather bound states in numerical scattering experiments.

ACKNOWLEDGMENTS

We acknowledge J. J. Mazo and J. L. Marín for many useful discussions on this work. Financial support is acknowledged to DGES PB98-1592 of Spain, also to MCyT and European Regional Development Fund (FEDER) program through BFM2002-00113 project. M.M. acknowledges financial support from the European Research Training Network (RTN) LOCNET HPRN-CT-1999-00163. L.M.F. acknowledges a Marie Curie Fellowship (cat. 40) HPMF-CT-2002-01965, and the hospitality of the Foundation of Research and Technology-Hellas, during the completion of this work.

[1] R. S. MacKay and S. Aubry, Nonlinearity **7**, 1623 (1994).
[2] S. Aubry, Physica D **103**, 201 (1997).
[3] J.-A. Sepulchre and R. S. MacKay, Nonlinearity **10**, 679 (1997).
[4] R. S. MacKay and J.-A. Sepulchre, Physica D **119**, 148 (1998).
[5] T. A. Kontorova and Ya. I. Frenkel, Zh. Eksp. Teor. Fiz. **8**, 1340 (1938).
[6] O. M. Braun and Yu. S. Kivshar, Phys. Rep. **306**, 1 (1998).
[7] L. M. Floría and J. J. Mazo, Adv. Phys. **45**, 505 (1996).
[8] J. L. Marín and S. Aubry, Nonlinearity **9**, 1501 (1996).
[9] E. Trías, J. J. Mazo, and T. P. Orlando, Phys. Rev. Lett. **84**, 741 (2000).
[10] P. Binder, D. Abraimov, A.-V. Ustinov, S. Flach, and Y. Zolotaryuk, Phys. Rev. Lett. **84**, 745 (2000).
[11] S. Takeno and M. Peyrard, Physica D **92**, 140 (1996).
[12] S. Takeno and M. Peyrard, Phys. Rev. E **55**, 1922 (1997).
[13] L. M. Floría, J. L. Marín, P. J. Martínez, F. Falo, and S. Aubry, Europhys. Lett. **36**, 539 (1996).
[14] P. Binder, D. Abraimov, and A. V. Ustinov, Phys. Rev. E **62**, 2858 (2000).
[15] L. M. Floría, J. L. Marín, S. Aubry, P. J. Martínez, F. Falo, and J. J. Mazo, Physica D **113**, 387 (1997).
[16] S. Watanabe, H. S. J. van der Zant, S. H. Strogatz, and T. Orlando, Physica D **97**, 429 (1996).
[17] V. I. Arnold, *Mathematical Methods of Classical Mechanics*, 2nd ed. (Springer, New York, 1989).
[18] J. L. Marín and S. Aubry, Physica D **119**, 163 (1998).
[19] S. Flach and M. Spicci, J. Phys.: Condens. Matter **11**, 321 (1999).
[20] J. L. Marín, F. Falo, P. J. Martínez, and L. M. Floría, Phys. Rev. E **63**, 066603 (2001).
[21] R. S. MacKay and J.-A. Sepulchre, J. Phys. A **35**, 3985 (2002).
[22] R. Boesch, P. Stancioff, and C. R. Willis, Phys. Rev. B **38**, 6713 (1988).

[23] S. Aubry and T. Cretegny, Physica D **119**, 34 (1998).
[24] D. Chen, S. Aubry, and G. Tsironis, Phys. Rev. Lett. **77**, 4776 (1996).
[25] P. J. Martínez, L. M. Floría, J. L. Marín, S. Aubry, and J. J. Mazo, Physica D **119**, 175 (1998).
[26] P. J. Martínez, L. M. Floría, F. Falo, and J. J. Mazo, Europhys. Lett. **45**, 444 (1999).
[27] J. X. Xu and J. Jiang, Chaos, Solitons Fractals **7**, 3 (1996).
[28] D. Bonart and J. B. Page, Phys. Rev. E **60**, R1134 (1999).
[29] R. S. Mackay, in *Stochastic and Spatial Structures of Dynamical Systems*, edited by S. J. van Strien and S. M. Verduyn Lunel (North–Holland, Amsterdam, 1996).
[30] S. Flach and K. Kladko, Physica D **127**, 61 (1999).
[31] H. J. Schnitzer, F. G. Mertens, and A. R. Bishop, Physica D **141**, 261 (2000).
[32] N. R. Quintero, A. Sánchez, and F. G. Mertens, Phys. Rev. E **62**, 5695 (2000).
[33] M. Meister, F. G. Mertens, and A. Sánchez, Eur. Phys. J. B **20**, 405 (2001).
[34] S. Flach and C. R. Willis, Phys. Rev. Lett. **72**, 1777 (1994).
[35] J.-A. Sepulchre, Proceedings of the El Escorial Conference (to be published).
[36] Recently changing F_{ac} we have found mode locked DB solutions with commensurate velocities [D. Zueco, P. J. Martínez, and F. Falo (in preparation)].